Microporous and Mesoporous Materials 272 (2018) 184–192

Contents lists available at ScienceDirect

Microporous and Mesoporous Materials

journal homepage: www.elsevier.com/locate/micromeso

A cheap mesoporous silica from fly ash as an outstanding adsorbent for sulfate in water

Ximena Castillo[a], Jaime Pizarro[a,*], Claudia Ortiz[b], Héctor Cid[b], Marcos Flores[c], Els De Canck[d], Pascal Van Der Voort[d]

[a] Departamento de Ingeniería Geográfica, Facultad de Ingeniería, Universidad de Santiago de Chile, Santiago, Chile
[b] Departamento de Biología, Facultad de Química y Biología, Universidad de Santiago de Chile, Santiago, Chile
[c] Departamento de Física, Facultad de Ciencias Físicas y Matemáticas, Universidad de Chile, Santiago, Chile
[d] Center for Ordered Materials, Organometallics & Catalysis (COMOC), Department of Chemistry, Ghent University, Ghent, Belgium

ARTICLE INFO

Keywords:
Fly ash
Sulfate
Mesoporous silica
Adsorption
Functionalization

ABSTRACT

This research describes the development of a very cheap mesoporous silica material similar to hexagonal mesoporous silica (HMS) and using a silicate extract as precursor. This precursor is obtained from cheap fly ash by an easy calcination process at 850 °C and a green extraction with water. The obtained mesoporous fly ash material had a surface area of 282 $m^2 g^{-1}$ and a pore size of 5.7 nm. It was functionalized with ethylene diamino moieties via the well-known SAMMS method, followed by a DRIFT analysis that clearly showed the successful functionalization. An excellent adsorbent was obtained for the adsorption of sulfate anions by the solid's modification with copper forming a copper-ethylenediamine complex. The adsorption of sulfates was studied in a batch system where the pH at highest adsorption 8 was and the adsorption time remarkably fast (5 min). The kinetic data were fitted according to a pseudo-second order model with a high coefficient of linear regression at different initial concentrations. The adsorption isotherm that best fitted the experimental data was the Freundlich model. The maximum sulfate adsorption capacity of this very cheap fly ash based adsorbent was 146.1 mg g^{-1}, 3 times greater than the values reported in literature and commercial adsorbent materials.

1. Introduction

The decreasing availability of water resources [1] due to contamination with heavy metals and oxoanions harmful to the human health [2,3] make it necessary to intensify the purification of industrial water so we can reuse it. The toxicity of oxoanions in relatively low concentrations such as chromates and arsenates is generally known [4,5]. In contrast, the oxoanion sulfate acts as a laxative [6] in a higher concentration range between 1000 and 2000 mg L^{-1}. As a result of industrial contamination, sulfates can cause serious environmental problems in several different forms: acid drainage in the mining industry [7,8] when tailings, effluents, and liquid slurries are poured into watercourses [9] and contamination during the use of natural water to cool thermoelectric plants [10]. The discharge of water with a high sulfate content into the environment also results in the salinization of the receiving ecosystems [11,12].

Several methods have been developed for capturing metals and oxoanions such as: ion exchange [13], chemical precipitation [14], osmosis [15] and membrane filtration. They are efficient removal technologies but most are very costly. Lower cost alternative methods have also been developed but unfortunately lack efficiency and specificity [16]. In contrast, the removal of these pollutants can also be performed via adsorption which is a cheaper and more selective technique. Mesoporous siliceous materials appear as highly efficient alternatives for the removal of polluting species [17] but their use is rather limited by the high cost of surfactants and precursors required in their synthesis [18]. There is an urgent need to develop lower cost alternative sources to be used as precursors and surfactants. Over the latest decades, there have been advances in the synthesis of the MCM-41 type of materials, using commercial silicates, fuming silica and silicates extracted from ash, those methods utilize strong alkaline solutions during synthesis generating residues difficult to dispose of [19,20]. In MCM-41, the formation of the structure occurs through strong electrostatic interactions which imply an inevitable calcination stage to remove the surfactant. This causes the loss of active surface, i.e., a decrease of available silanol functions and consequently, a decrease of chemical anchoring possibilities when using grafting procedures [21].

The objective of this study is the development of a hexagonal

* Corresponding author.
E-mail address: jaime.pizarro@usach.cl (J. Pizarro).

https://doi.org/10.1016/j.micromeso.2018.06.014
Received 26 March 2018; Received in revised form 28 May 2018; Accepted 7 June 2018
Available online 15 June 2018
1387-1811/

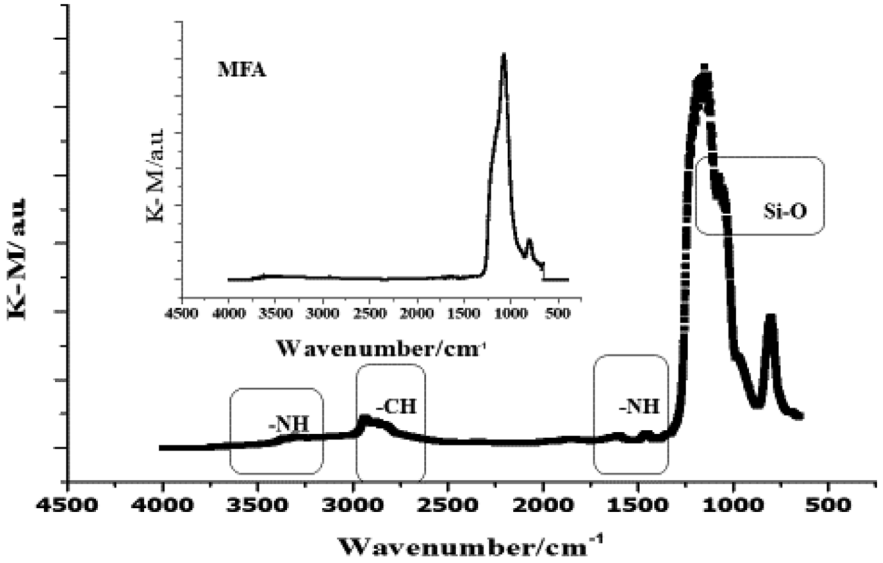

Fig. 1. a) DRIFT spectrum of MFAEDA. b) DRIFT spectrum of MFA before the functionalization with 1-(2-aminoethyl)-3-aminopropyl trimethoxysilane.

Table 1
Textural parameters and elemental analysis of MFA and MFAEDACu materials.

Sample	Pore size (BJH) (nm)	Surface area (BET) (m^2g^{-1})	Pore volume (cm^3g^{-1})	N (mmol g^{-1})	C (mmol g^{-1})	Cu[a] (mmol g^{-1})	N/Cu
MFA	5.7	281.7	0.41	–	0.25	–	–
MFAEDACu	3.4	126.7	0.19	1.97	6.7	4.3	0.5

[a] Value determined by ICP.

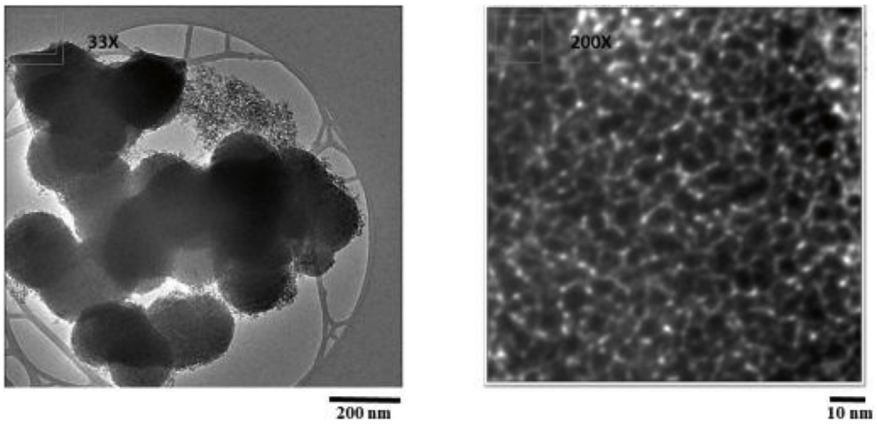

Fig. 2. TEM image of MFA. Left: 33X. Right: 200X.

mesoporous silica type of material (HMS) using a silica source extracted from cheap fly ash serving as precursor of the mesoporous structure. The synthesis procedure avoids expensive surfactants. The framework is formed via weak hydrogen bond interactions that also allow an easy removal of the surfactant by solvent extraction, yielding a greater density of active groups (i.e. silanols) on the surface and the formation of thicker walls with greater thermal stability [22]. Furthermore, the siliceous extract replaces the commercial silica precursors and is obtained by a less polluting method [23]. Once the structure has been formed, it is functionalized with an ethylenediamine (EDA) copper complex by the SAMMS method [24] for an in-depth sulfate adsorption study.

2. Materials and methods

2.1. Reagents

All the reagents were analytical graded and of Suprapur quality. They were used as received without any further purification and are listed next: Dodecylamine (DDA, Merck), 1-(2-aminoethyl)-3-aminopropyl trimethoxysilane (APTMS, 98%, Aldrich), calcium carbonate (Na_2CO_3, Merck), copper (II) chloride ($CuCl_2$ $2H_2O$, Merck), sodium sulfate (Na_2SO_4, Sigma Aldrich), absolute ethanol (CH_3CH_2OH, Merck), toluene ($C_6H_5CH_3$, Merck), 2-propanol ($CH_3CHOH(CH_3)$, Merck). The solutions were prepared using MilliQ water (Millipore, Synergy uv). The pH adjustment was made with 0.1 M NaOH and 0.1 M HNO_3 solutions.

The fly ash in this study was of class F and was obtained from a burning coal power plant located in Valparaiso, Chile.

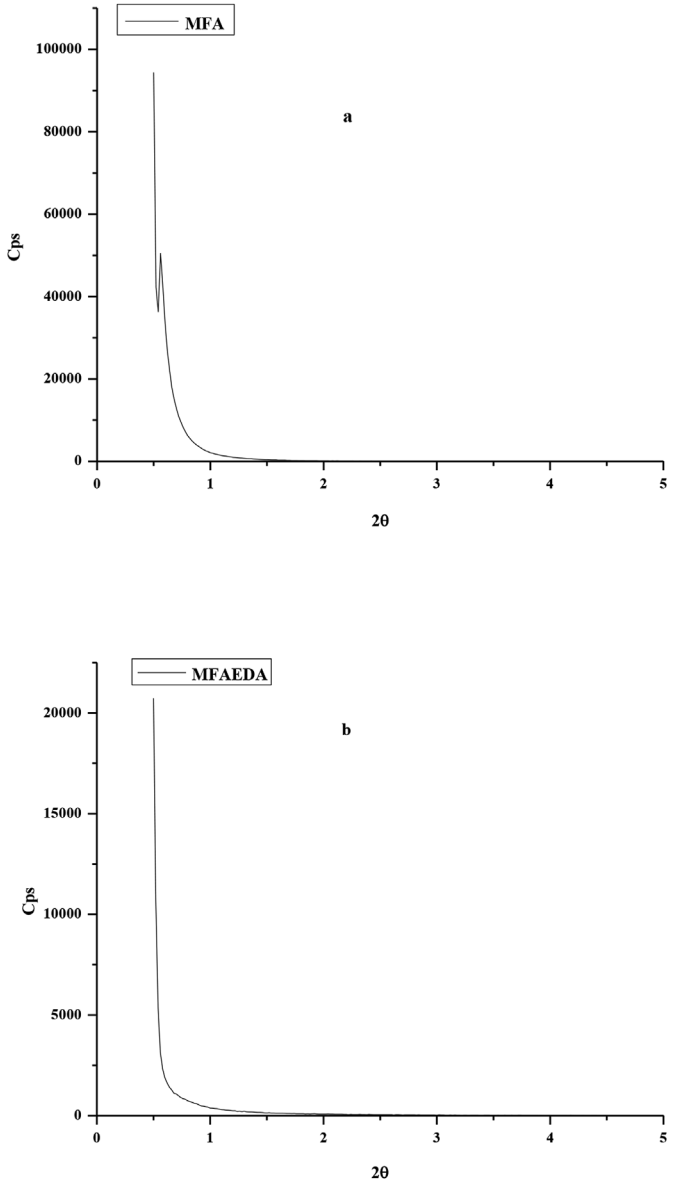

Fig. 3. X-ray diffraction pattern. a) MFA. b) MFAEDA.

2.2. Synthesis of the adsorbing material, MFAEDACu

The synthesis of the copper containing mesoporous material (MFAEDACu) was carried out in four stages: (1) extraction of silicates from fly ash which are used as silicon source, (2) synthesis of mesoporous silica material (mesoporous fly ash; MFA), (3) modification of MFA with an ethylenediamine (EDA) functionality via grafting of a silane (MFAEDA), and (4) formation of the Cu(II) complex on the functionalized material (MFAEDACu). The first stage consisted of the extraction of soluble silicates from fly ash by calcination at 850 °C with sodium carbonate for 2.5 h, followed by treatment with water [23]. Once the elemental composition of the extract had been determined via ICP-MS, MFA was synthesized using a modified method [22] where the inorganic precursor (I°) tetraethyl orthosilicate (TEOS) was replaced by the extracted silicate; using dodecylamine (S°) (DDA) as surfactant in an I°/S° = 4.5 Molar ratio. To remove the template, the material was Soxhlet extracted using ethanol over a period of 5 h. The third stage consisted of the functionalization of MFA by the self-assembly technique on the mesoporous material (SAMMS) with 1-(2-aminoethyl)-3-aminopropyl trimethoxysilane (APTMS) [24]. This included the rehydroxylation of the surface of MFA with 2.5 monolayers of water under constant stirring during 1 h at ambient temperature and in a toluene suspension. Then, a certain amount of the functionalizing agent, APTMS, was added to this suspension to obtain a monolayer and was kept under reflux for 6 h to be distilled afterwards. The functionalized material, MFAEDA, was recovered by vacuum filtration, washed with 2-propanol, and dried. In the fourth stage, the MFAEDA was treated with an aqueous solution of $CuCl_2$, washed, and dried to yield MFAEDACu. To ensure that MFAEDACu did not contain any water, the solid was refluxed in toluene equipped with a Dean-Stark trap for 2 h, washed with 2-propanol, and dried [25].

2.3. Characterization

The determination of the morphology and porous network of MFA and MFAEDACu was performed by Electron Transmission Microscopy (TEM) and X-ray Diffraction (XRD), respectively; the study of the superficial chemistry of both materials, before and after the functionalization, was carried out by Fourier Transform Diffuse Reflectance Spectroscopy (DRIFT) and X-ray Photoelectronic Spectroscopy (XPS); determination of the surface area, pore size distribution and chemical composition (CHNS) were made by Brunauer-Emmett-Teller method (BET), Barrer, Joyner and Halenda method (BJH) and Elemental Analysis, respectively.

Nitrogen adsorption-desorption was performed at 77 K using a Micromeritics Tristar 3000 gas analyzer. The samples were degasified at 120 °C for 12 h before the measurement. The surface area (S_{BET}) was measured using the BET method and the pore volume (V_p) was determined at $P/P_0 = 0.98$. The pore size of the materials ($d_{p,BJH}$) was obtained using the BJH method on the adsorption branch. The structure and morphology were characterized using TEM on a Hitachi TEM System at 120 KV, X-ray diffraction (XRD) with an ARL X'TRA diffractometer with 0.15418 nm wavelength Cu Kα radiation, and a solid-state detector. The quantification of amines was made by CHNS elemental analysis in a Thermo Flash 2000 elemental analyzer using V_2O_5 as catalyst. The examination of the amino groups of the functionalized material was performed by DRIFT spectroscopy on a Thermo Scientific Nicolet 6700 apparatus with a MCT detector cooled with liquid nitrogen. A Specac DRIFT cell made it possible to measure at 120 °C under vacuum. The study of the materials' surface modification before and after the adsorption of sulfates was performed by XPS on a Model PHI 1257 Perkin-Elmer XPS-Auger electron spectrometer with a hemispherical electron analyzer running under ultrahigh vacuum at 10^{-7} mbar, with an unfiltered Kα radiation X-ray source from an Al anode ($h\nu = 1486$ eV), an emission angle of 90° (normal emission), spectra calibrated with C1s carbon, and adventitious signals at a binding energy of 284.8 eV. The analyzed samples were in powder form, arranged 10 mm × 10 mm without prior treatment, and inserted in the analysis chamber.

2.4. Adsorption studies

The tests were performed using a batch method, directly mixing the mesoporous adsorbent material, MFAEDACu, with standard solutions of sodium sulfate [4]. The samples were stirred at ambient temperature at 150 rpm for the time corresponding to the analysis, then filtered (pore size of 0.2 μm) and analyzed at 500 nm by turbidimetric technique with a UV-VIS spectrophotometer (Ray Leigh UV-160). The following parameters were altered to study the adsorption process in-depth: pH, equilibrium time, adsorbent/adsorbate ratio, initial sulfate concentration and maximum load. The effect of pH on the sulfate adsorption of MFAEDACu was analyzed using 5 mL of solution of 1000 mg L^{-1} sulfate with 0.1 g of MFAEDACu, adjusting the pH between 2 and 8 using HNO_3 and NaOH, to determine the optimum pH value corresponding to maximum adsorption. The equilibrium time was determined using 0.1 g of MFAEDACu in 5 mL sulfate solutions with concentrations of 160,

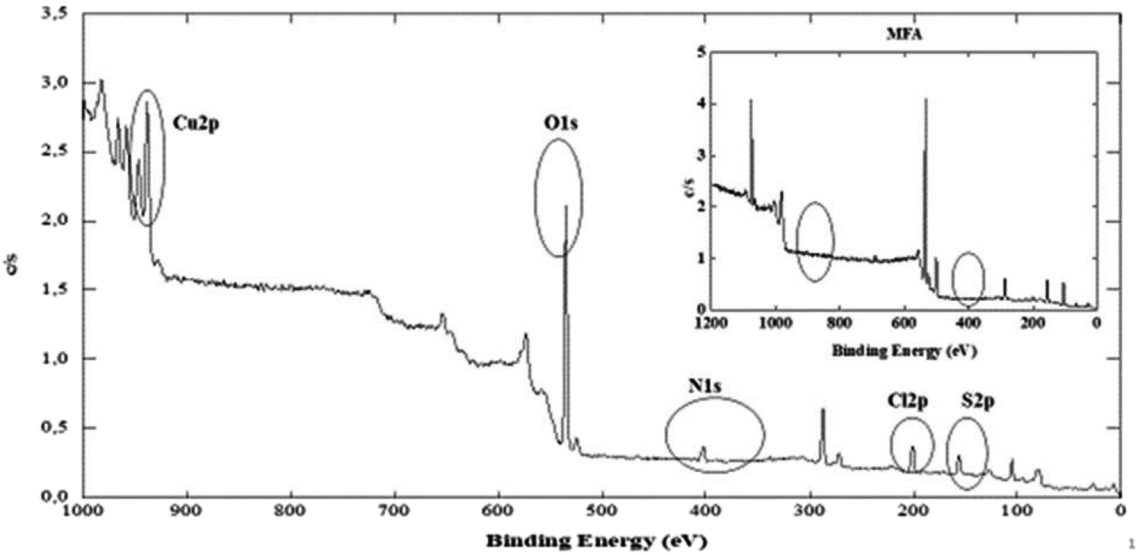

Fig. 4. A) Full range spectrum of MFAEDACu after the adsorption of sulfate at a concentration of 1000 mg L^{-1}, pH = 8.5 min b) MFA before functionalizing.

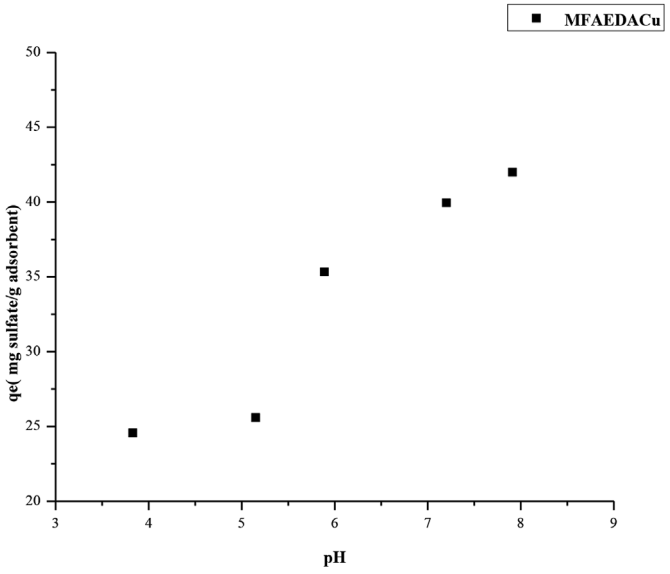

Fig. 5. Effect of pH on the adsorption of sulfate on 0.1 g of MFAEDACu from 5 mL of 1000 mg L^{-1} sulfate solution and 5 min of constant stirring (150 rpm).

380, 700, and 975 mg L^{-1} under constant stirring (150 rpm) and at ambient temperature at intervals of 5, 10, 20, 40, and 60 min at the optimum pH determined. The effect of the initial concentration was studied from a mixture of 0.1 g of MFAEDACu and 5 mL sulfate solution at concentrations of 47–1250 mg L^{-1}, under constant stirring (150 rpm). Ten adsorption tests were executed with MFAEDACu to determine the maximum load, contacting 0.1 g of MFAEDACu with 5, 10, and 25 mL of the 1240 mg L^{-1} sulfate solution at the maximum adsorption pH during 5 min. The sulfate removal efficiency (R_e, %) of MFAEDACu in the adsorption tests was calculated using the equation below (1):

$$R_e = \frac{C_o - C_e}{C_o} \times 100\ \% \quad (1)$$

where C_o is the initial adsorbate concentration in the solution (mg L^{-1}), and C_e is the concentration of adsorbate in the solution at equilibrium (mg L^{-1}). The adsorption capacity at equilibrium, q_e, was calculated from equation (2),

$$q_e = \frac{(C_o - C_e) \times V}{W} \quad (2)$$

where V is the volume of the solution (mL), and W is the mass of adsorbent (g).

Sulfate concentration range used in the tests was to simulate the industrial wastewater treatment.

3. Results and discussion

3.1. Characterization of MFAEDACu

The DRIFT analysis of MFAEDACu is shown in Fig. 1. The spectrum of the pristine MFA material shows intense signals at 1100 cm^{-1} and 800 cm^{-1} that correspond to the symmetric and asymmetric Si-O stretching vibrations respectively and can be attributed to the siloxane bonds (Si-O-Si) in the mesoporous network (this signal would account for the formation of the network). A small but sharp signal at 3700 cm^{-1} is also observed that corresponds to the silanol group (Si-OH) (the functionalizing agent is grafted on the silanol group) [26,27]. Although no peaks of the surfactant DDA are observed in the spectrum, the MFA elemental analysis results point to the presence of a small amount of C (0.25 mmol g^{-1}, Table 1). After functionalization with APTMS, signals in the 2800-2900 cm^{-1} range appear that can be attributed to C-H stretching vibrations of the propyl and ethyl chains in the functionalization agent. It is not excluded that signal could also be influenced by C-H of methoxy groups; the C-O in the methoxy group should emit a signal within the range of 1333–1022 cm^{-1}, however, based on Fig. 1, this signal cannot be identified since it possible overlapped with that of the Si-O group and would be responsible for the signal's observed widening Furthermore, a small signal at 3300 cm^{-1} is seen that corresponds to an N-H stretching vibration of the amino groups [26]. The presence of these groups is also confirmed by the N-H bending vibration bands that appear in the 1500-1600 cm^{-1} region [28]. The amino group allows the formation of the complex CuEDA. The signal of the silanols at 3700 cm^{-1} disappears completely after functionalization with APTMS, indicating a successful functionalization.

Table 1 shows the results of the nitrogen adsorption-desorption analysis and the pore size distribution of the MFA before and after modification. The isotherms are of type IV and are characteristic for a mesoporous structure [37] with H3 hysteresis loop class (characteristic of pores in the form of canals or slits) at P/P_0 from 0.4 to 0.98 value indicate of Material of high textural mesoporosity, desirable in

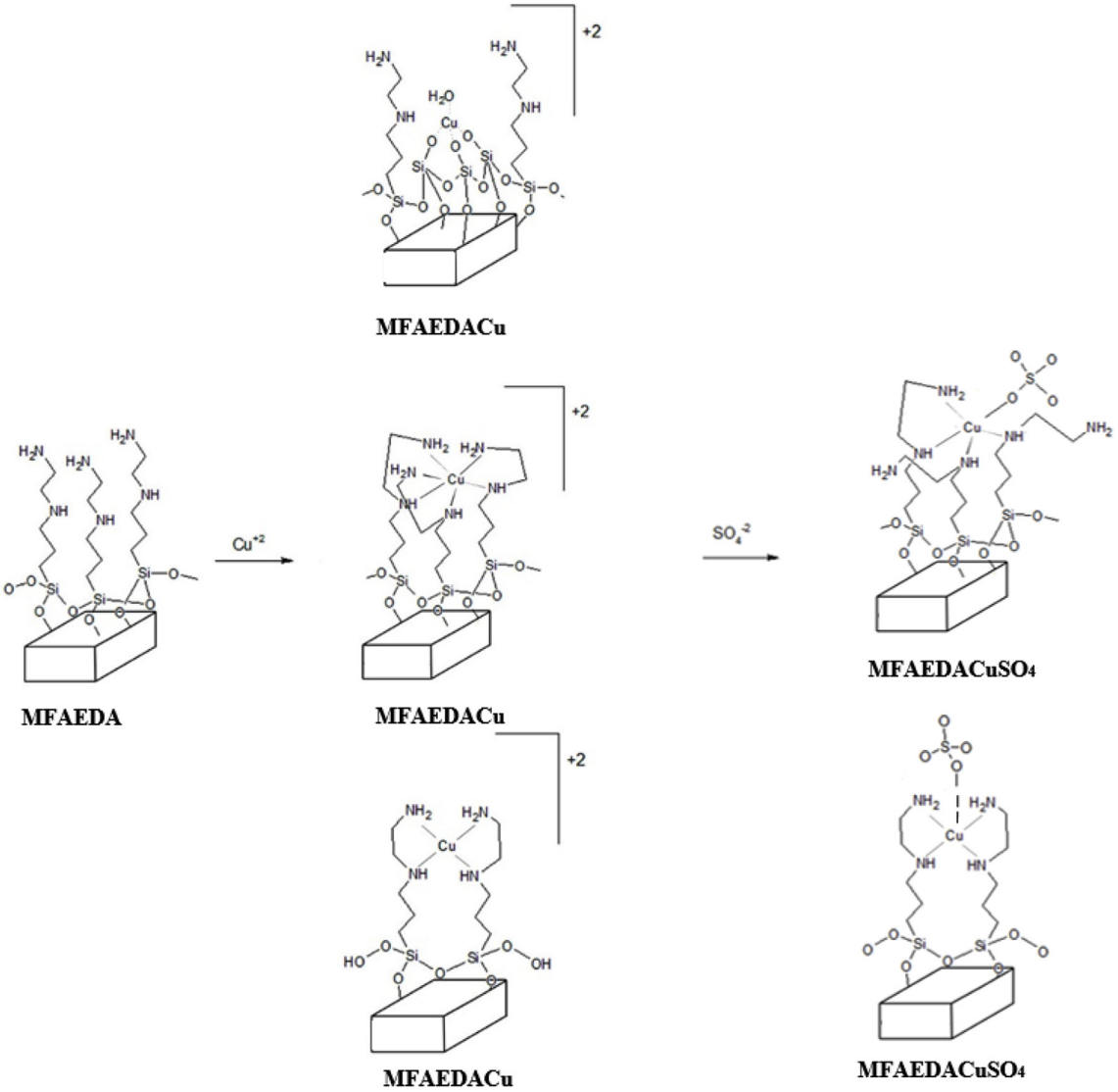

Scheme 1. Depiction of the modification of MFAEDA through metal ion chelation and adsorption of sulfate.

adsorbent materials [21]. The synthesis with the fly ash precursor and DDA surfactant thus resulted in a porous material with high surface area, mesopores and a relatively large pore volume. After functionalization with APTMS and copper, a general and expected decrease was measured of the surface area ($282\,m^2\,g^{-1}$ to $127\,m^2\,g^{-1}$), pore size (5.7–3.4 nm), and pore volume ($0.41–0.19\,cm^3\,g^{-1}$). This is due to the decoration of the pore walls with the functionalization and the addition of weight which in turn confirms that MFA was successfully modified towards MFAEDACu.

Fig. 2 shows the TEM analysis of MFA, with the diameter of the cavities ranging from 4 to 8 nm (picture on the right) in agreement with the nitrogen sorption analysis of the material (Table 1).

Fig. 3a and b shows the results of the X-ray diffraction analysis of MFA and MFAEDA. A reflection in the region corresponding to $2\theta = 0$-1° was observed in the diffractogram of the material before modification (Fig. 3a), yet disappeared after the functionalization (Fig. 3b). In HMS-type materials, it is common to find a single wide signal at approximately $2\theta = 2^\circ$ associated with the (100) plane, but these materials can have a short range hexagonal order which is not dissolved in this analysis [29]. The disorder and small domains are explained by the weak interaction forces (hydrogen bonds) of the amine that make up the material and are used as surfactant and inorganic precursor, in our synthesis corresponding to the silicates extract obtained from the ashes as precursor [29].

Table 1 moreover presents the C and N elemental composition of MFA and MFAEDACu. MFA contains a small amount ($0.25\,mmol\,g^{-1}$) of C that probably comes from a small DDA fraction that was not extracted during the template's elimination step. A clear increase in C and N content after functionalization can be seen, originating from the functionalization agent (APTMS) in MFAEDACu. The expected stoichiometric C:N ratio after the entire functionalization process should be 5C:2 N [30]; however the excess $1.6\,mmol\,g^{-1}$ is found can be attributed to methoxy groups of the functionalizing agent which were not extracted in the distillation.

Fig. 4a and b shows the results of the solid's XPS analysis after sulfate adsorption, MFAEDACu-SO_4^{-2}, and MFA. Fig. 4b shows signals at 530 eV and 100 eV, which can be attributed to O1s and Si2p respectively. These signals probably correspond to the siloxane groups of the mesoporous network. Fig. 4a shows a clear signal at 400 eV, attributable to the N groups from the functionalization [31]; a signal not observed in the non-functionalized material MFA (Fig. 4b). The signals at 935 eV and 200 eV can be ascribed to Cu2p [25,32] and Cl2p [33] respectively, which correspond to the formation of the Cu complex from $CuCl_2$, on the functionalized material. Finally, the signal at 169 eV can be assigned to S2p, confirming the linkage of sulfates with MFAEDACu [34].

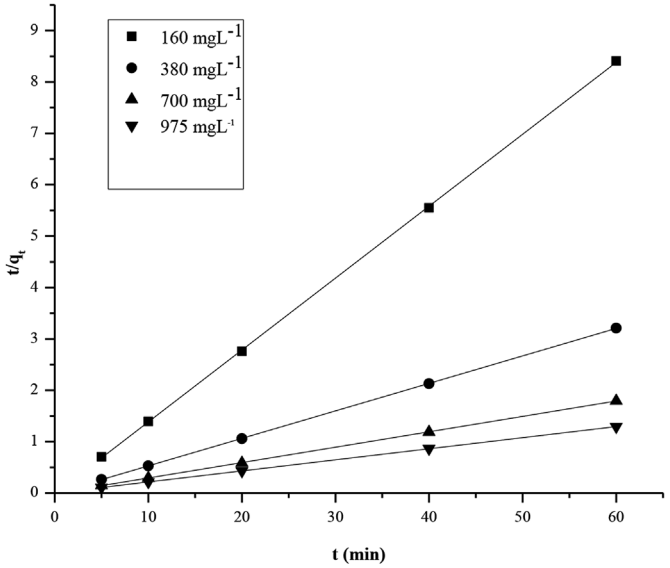

Fig. 6. Fitting of experimental data to pseudo-second order kinetics model, with 0.1 g of MFAEDACu adsorbent, 5 mL of sulfate solution at concentrations of 160, 380, 700, and 975 mg L^{-1}, with constant stirring (150 rpm) at ambient temperature and at 5, 10, 20, 40, and 60 min intervals, pH = 8.0.

Table 2
Adsorption parameters of the Langmuir and Freundlich models obtained from the fitting of the experimental data of sulfate adsorption on MFAEDACu.

Species	Langmuir model					Freundlich model	
	q_L (mg g^{-1})	K_L (L mg^{-1})	R_L	R^2	n	K_F (mg g^{-1}) (mg $L^{-1})^{1/n}$	R^2
SO_4^{-2}	138.889	0.002	0.103	0.9999	1.070	0.334	0.9998

Table 3
Pseudo-second order kinetic adsorption parameters obtained by fitting the experimental sulfate adsorption data on MFAEDACu.

C_o (mgL^{-1})	k_2 (g$mg^{-1}min^{-1}$)	R^2	q_e, cal (mgg^{-1})	q_e, exp (mgg^{-1})	SEE (q_e)
160.0	1.2	0.9999	7.1	7.3	0.01
380.0	0.4	0.9999	18.7	18.9	0.04
700.0	0.1	0.9999	33.3	34.1	0.51
975.0	11.7	0.9999	46.3	46.7	0.16

3.2. Adsorption studies

3.2.1. Effect of pH

Fig. 5 shows the results of the sulfate adsorption on MFAEDACu at different pH values. The highest sulfate adsorption is found within the pH 6.0–8.0 range, varying between 57% and 68% of sulfate capture (35–42 mg g^{-1}). In this pH range, the SO_4^{-2} anion is free and its removal from the solution by the adsorbent may be attributed to:

- The possible displacement of the labile ethylene diamino ligands from the octahedral copper ethylenediamino complex MFAEDACu [35] could allow a change in copper cation coordination number from 6 to 5, and/or;
- Sulfate group binding to the $Cu(EDA)_2$ complex according to Scheme 1.

The electrostatic interaction of sulfate with groups carrying a positive charge cannot be discarded [36] (e.g. amino groups) since the

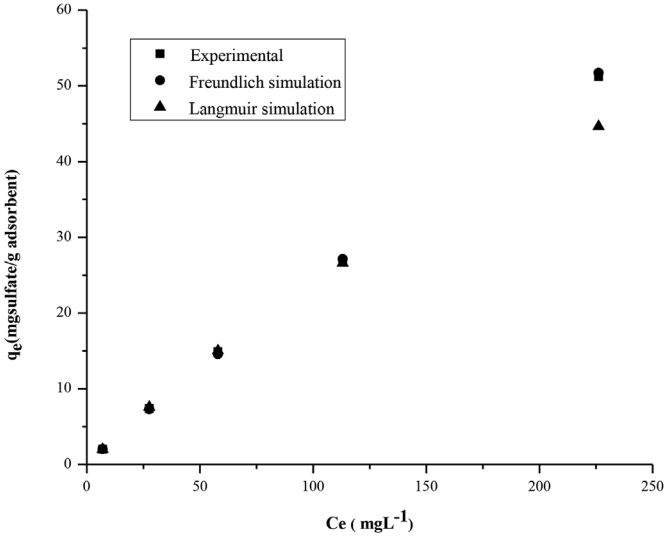

Fig. 7. Comparison equilibrium adsorption capacity (qe). Experimental, Freundlich and Langmuir simulation. Experimental data obtained from adsorption tests with 0.1 g of MFAEDACu constant stirring (150 rpm) 5 min; 5 mL of sulfate solutions in concentrations of 47, 175, 356, 650, and 1250 mg L^{-1}; pH = 8.0.

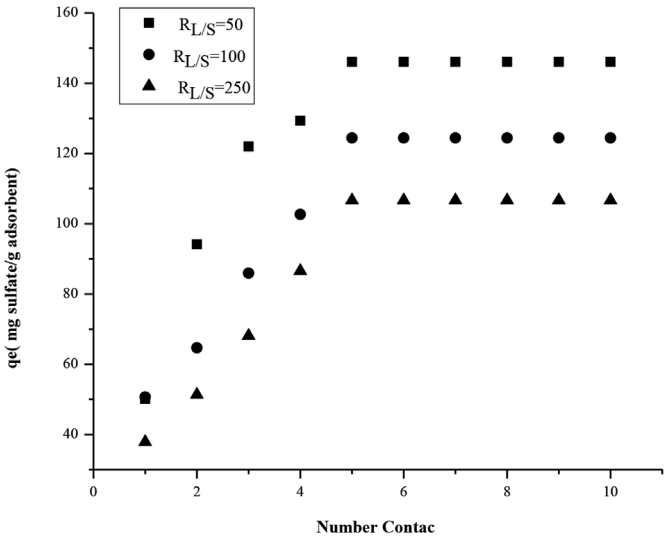

Fig. 8. Maximum load capacity study. Ten adsorption tests were carried out on MFAEDACu, contacting 0.1 g of MFAEDACu with 5, 10, and 25 mL of 1240 mg L^{-1} sulfate solutions at pH = 8.0 during 5 min with constant stirring (150 rpm).

pH_{final} in the adsorption tests is ≈ 4.0.

3.2.2. Adsorption kinetics

The maximum adsorption concentration at equilibrium was reached between 5 and 10 min, at different concentrations r of 160, 380, 700, and 975 mg·L^{-1} (R_e % = 82, 96, 81, and 45%, respectively). These results confirm that MFAEDACu possesses a fast sulfate adsorption capacity and that diffusion of species in the pores of the mesoporous material is not a limiting factor in the capture process [24].

The experimental data allowed the fitting of a pseudo-second order kinetic model [37] which is represented by the linearized Eq. (3.1):

$$\frac{t}{q_t} = \frac{1}{k_2 \cdot q_e^2} + \frac{t}{q_e} \quad (3.1)$$

where k_2 is the pseudo-second order rate constant (g mg^{-1} min^{-1}) and q_e is obtained from the slope and the intercept of the t/q_t vs. t curve

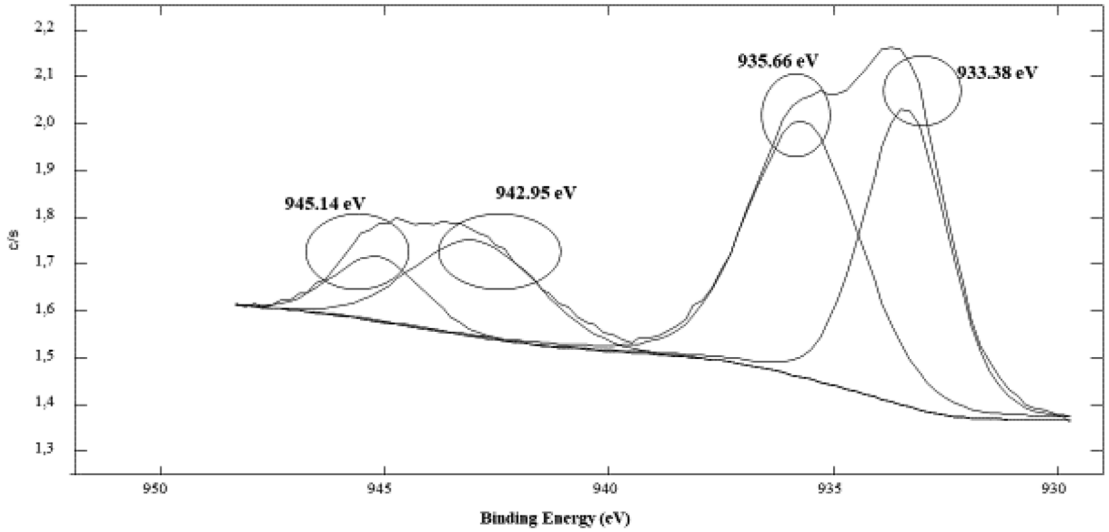

Fig. 9. High resolution spectrum of Cu2p of MFAEDACu before the adsorption of sulfate.

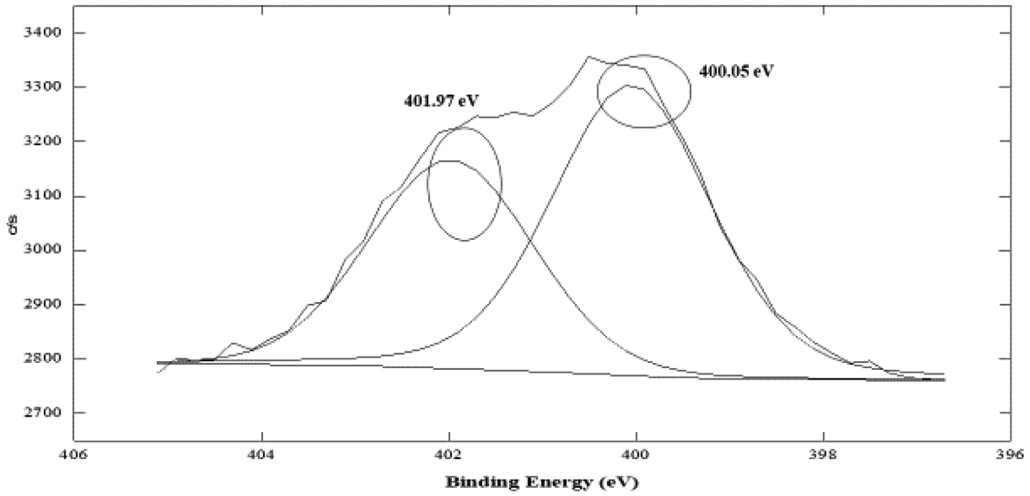

Fig. 10. High resolution XPS spectrum of N1s of MFAEDACu before the adsorption of sulfate.

(Fig. 6; Table 2).

The results of the fitted model (Table 2) show the correlation coefficient (R^2). The values of q_e calculated from the model lie very closely to the experimental data, suggesting a chemisorption process [38] for the sulfate capture by the synthesized material.

The sum of the square of the errors (SEE), is give as (Eq. (3.2)):

$$\mathbf{SSE}= \sum_{i=1}^{n} \left(q_{e,estm} - q_{e,exp}\right)_i^2 \tag{3.2}$$

Where, $q_{e,}$ estm and $q_{e,exp}$ are, respectively, the estimated and the experimental value of the equilibrium adsorbate solid concentration in the solid phase (mg/g), and n is the number of the data point (Table 3).

3.2.3. Adsorption isotherms

Fig. 7 shows the equilibrium concentration (C_e) vs. the specific adsorption capacity (q_e). It is seen that q_e increases with an increasing C_e. The experimental equilibrium data were fitted to the Langmuir and Freundlich models (Table 3). The Langmuir isotherm describes the adsorption phenomenon in which the adsorbing solid has a limited adsorption capacity designated by q_L, forming a monolayer on a homogenous surface without interaction between the adsorbed molecules [39]. The linearized equation of the Langmuir's isotherm is expressed as (Eq. (4.1)):

$$\frac{C_e}{q_e} = \frac{1}{q_L \cdot K_L} + \frac{C_e}{q_L} \tag{4.1}$$

Where q_e is the adsorption capacity of the adsorbent at equilibrium (mg g^{-1}), K_L is the Langmuir's adsorption constant (L mg^{-1}) associated with the adsorption affinity between adsorbent and adsorbate, and q_L is the adsorbent's maximum adsorption capacity when forming the monolayer (mg g^{-1}).

Eq. (4.2) represents a dimensionless factor that describes the nature of the adsorption process, in such a way that $R_L = 0$ indicates irreversible adsorption; $0 < R_L < 1$, a favorable adsorption; $R_L = 1$, a linear adsorption, and $R_L > 1$ unfavorable adsorption [39], where C_i is the initial concentration:

$$R_L = \frac{1}{1 + K_L C_i} \tag{4.2}$$

The Freundlich's isotherm on the other hand is applied to nonideal adsorption processes on heterogeneous surfaces, and the model's linearized equation is represented by

$$\ln(q_e) = \ln(K_F) + \frac{1}{n} \cdot \ln(C_e) \tag{5}$$

where K_F (mg g^{-1}) (L $mg^{-1})^{1/n}$ is Freundlich's constant related to the adsorption capacity and n to the adsorption intensity (Table 3).

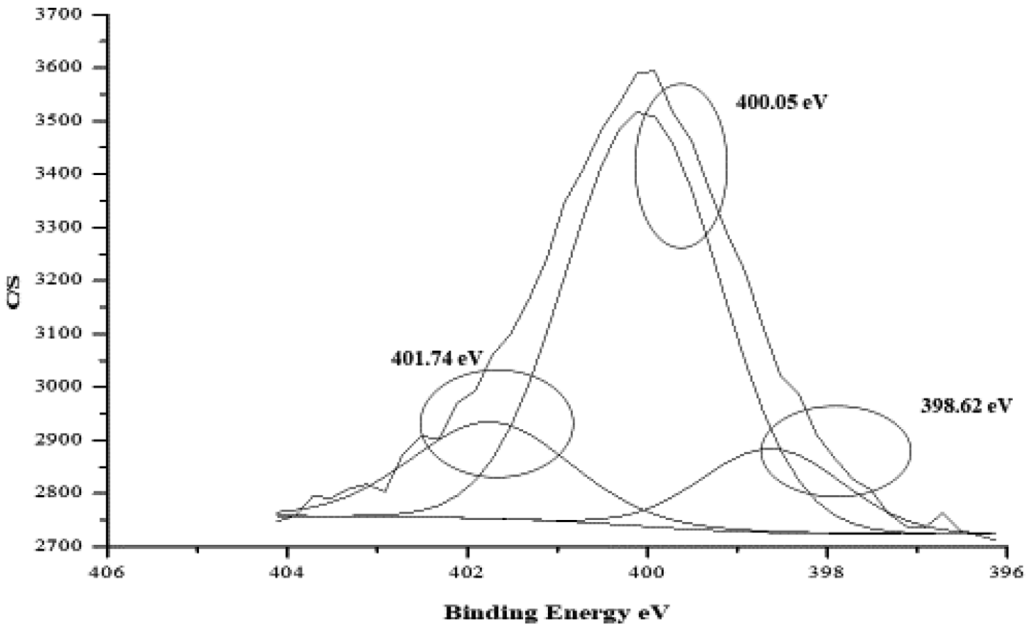

Fig. 11. High resolution XPS spectrum of N1s of MFAEDACu after the adsorption of sulfate at a concentration of 1000 mg L^{-1}; pH = 8; 5 min; constant stirring (150 rpm).

A good correlation coefficient was determined from the fitting of the experimental data with both models (Table 3); however, looking at the maximum load q_L in Langmuir's model (138.89 mg g^{-1}), it turns out to be smaller than the value obtained in the maximum adsorption load tests, q_{max} = 146.1 mg g^{-1} (Fig. 8). Comparing the value of q_e calculated for Langmuir's model with the experimental value q_e, the estimation is smaller. If this comparison is made with Freundlich's model, the estimation of q_e has a better fit (Fig. 7). These results suggest that the Freundlich model is the one that best represents the sulfate's adsorption process on the fly ash based adsorbent.

The most commonly used industrial technique for the treatment of sulfate-contaminated water is lime precipitation [9]. Over the last few decades, the development of adsorbent materials has also allowed for the adsorption of oxoanions in which the species of greatest interest are chromate, arsenate, selenate and molybdate [36] and more recently phosphate [36]. The ability to capture sulfate in mesoporous materials has however only been studied when sulfate was used as competing anion together with the oxoanions mentioned above [36].

When comparing the adsorption capacity of the mesoporous material in this study (146.1 mg of sulfate g^{-1}) with mesoporous materials functionalized with a similar Cu-EDA complex for the adsorption of phosphate [42], it can be concluded that our material has an oxoanion adsorption capacity that is 3 times greater than the capacity reported in the literature. Only 43.3 mg $PO_4^{-3} g^{-1}$ could be adsorbed although both anions are very similar with respect to the bond length between the central atom and oxygen, i.e., r (SO) = 0.148 nm (SO_4^{-2}) and r (PO) = 0.154 nm (PO_4^{-3}) [42]. Other mesoporous materials functionalized with Fe-EDA and La-EDA complexes [36] and the commercial material zirconium ferrite [42] showed significantly lower adsorption capacities (51.84 mg g^{-1}, 54.72 mg g^{-1} and 39.8 mg g^{-1}, respectively) in comparison to our material.

3.2.4. Adsorption mechanism

The elemental analysis of the sulfate adsorbed on MFAEDACu has an N/Cu ratio = 0.5 (Table 1). When comparing this result with that expected for the formation of the $Cu(EDA)_3$ complex, one can find a ratio of ≥3.5 [40–42]; this suggests that even though the Cu(II)EDA complex was formed, a fraction of Cu(II) can be bound to residual silanol groups on the surface of the material as suggested in Scheme 1 [40]. Another aspect that allows us to determine the presence of the Cu $(EDA)_3$ complex is the density of surface EDA groups, whose value should be greater than or equal to 3.0 EDA nm^{-2}. It was established via elemental analysis that the material in this study has a density of 2.1 EDA nm^{-2}. This result might suggest the formation of complexes such as $Cu(EDA)_2Cl_n^{-1}$ and $Cu(EDA)Cl_n^{-1}$ [40]. The XPS analysis indicates that Cl 2p [33] is present in MFAEDACu. Additionally, the experimental adsorption results show that the maximum adsorption capacity (Fig. 8) was 146.1 mg g^{-1}, a value four and a half times greater than the expected value, if only the formation of the $Cu(EDA)_3$ complex is considered. The elemental analysis (Table 1) allows the estimation of the formation stoichiometry of the $Cu(EDA)_3$ complex. Every EDA group has 2 N (0.99 mmol g^{-1}). The formation of the complex requires a 3:1 stoichiometry (3 EDA:Cu) [4,25,35,41], i.e., 0.33 mmol g^{-1} of the complex would be formed on the material, and since it is expected that the complex should capture sulfate in a 1:1 ratio, the capacity for removing sulfate anions would be 0.33 mmol g^{-1}, or 32 mg of sulfate per gram. Comparable results have been obtained with other materials [40].

The analysis of the high-resolution spectrum of Cu2p of MFAEDACu (Fig. 9) before the sulfate adsorption shows two signals at 933.38 and 935.66 eV, in addition to the signals at 942.95 and 945.14 eV. It has been reported [32] that Cu(II) shows signals in the 934 eV region, and satellite peaks in the 944 eV region. Furthermore, it has been reported [43] that the signal of Cu(II) is displaced according to its chemical environment. Tetrahedral environments would shift the signal to higher energy values, while on the other hand octahedral environments would displace it to lower energies [43]. This allows us to state that the signals seen for Cu2p could be due to the coordination of Cu and N coming from the functionalization with EDA of the synthesized material, allowing the formation of mono-, di- or multidentate Cu complexes with N [32].

Analysis of the high-resolution spectra of N1s (Fig. 10) of MFAEDACu before the sulfate adsorption allows for the identification of two signals at 400.05 and 401.97 eV, which originate from free amino groups and protonated amines respectively, of the EDA ligand used in the functionalization [44]. After the adsorption of sulfate, three signals are seen at 398.62, 400.05, and 401.74 eV (Fig. 11). The 398.62 eV signal, which is absent in the N1s spectrum (Fig. 10), can be attributed to the opening of the EDA chains after sulfate adsorption [45]. On the other hand, the decrease in intensity of the signal at 401.74 eV,

assigned to protonated amines, would indicate that the sulfate anions can be adsorbed through electrostatic interactions in these groups with positive density.

4. Conclusion

The soluble silicates extracted from cheap fly ash allowed for straightforward synthesis of the mesoporous material, MFA, without the use of expensive surfactants yet with an easy work-up. A specific surface area of 282 $m^2 g^{-1}$ was obtained with a pore size of 5.7 nm. The synthesis of this material represents a promising alternative that replaces synthetic reagents in the development of mesoporous materials for industrial applications. The functionalization of MFA with ethylene diamino functionalities towards MFAEDA was successful and confirmed by DRIFT analysis. Additional functionalization with copper resulted in a suitable adsorbent for sulfate.

The N/cation ratio, the density of the functionalizing agent, and the result of the XPS analysis suggest the formation of Cu(II) complexes on the functionalized material, MFAEDACu, such as $Cu(EDA)2Cl_n^{-1}$, $Cu(EDA)Cl_n^{-1}$, and $Cu(EDA)_3$.

The adsorption of sulfate on the functionalized material depends on pH. The maximum sulfate adsorption capacity was 146.1 mg g^{-1} and the adsorption kinetics agreed with a pseudo-second order model whose adsorption isotherm fits the Freundlich model. The adsorbent showed a higher adsorption capacity compared to other adsorbents reported in literature.

Acknowledgements

The authors would like to acknowledge Ghent University for financial support. We are also very grateful to Funda Aliç from Ghent University for assistance in the laboratory and elemental analysis measurements. Ximena Castillo acknowledges to CONICYT (National Commission for Scientific Research and Technology) for financial support (grant N° 21140403). Conicyt grant N° ACT1410 and Dicyt grant N° 0921640PK.

References

[1] A. Hoekstra, M. Mekonnen, A. Chapagain, R. Mathews, B. Richter, PLoS One 7 (2012) e32688, http://dx.doi.org/10.1371/journal.pone.0032688 2012 , Accessed date: 5 May 2016.
[2] J. Weis, P. Weis, Environ. Int. 30 (2004) 685–700.
[3] L. Jarup, Br. Med. Bull. 68 (2003) 167–182.
[4] G. Fryxell, J. Liu, T. Hauser, Z. Nie, K.F. Ferris, S. Mattigod, M. Gong, R. Hallen, Chem. Mater. 11 (1999) 2148–2154.
[5] H. Yoshitake, T. Yokoi, T. Tatsumi, Chem. Mater. 14 (2002) 4603–4610 Centre for Disease Control and Prevention. Health Effects from Exposure to Sulfate in Drinking water workshop. Environmental Protection Agency https://nepis.epa.gov/ , Accessed date: 9 September 20171999.
[6] J. Skousen, C. Zipper, A. Rose, P. Ziemkiewicz, R. Nair, L. McDonal, R. Kleinmann, Mine Water Environ. 36 (2017) 133–153.
[7] S. Al-Abed, P. Pinto, J. Mackernan, E. Feld-Cook, S. Lomnicki, Chem. Eng. J. 323 (2017) 270–277.
[8] S. Venalainen, H. Hartikainen, Sci. Total Environ. 599 (2017) 1608–1613.
[9] Z. Henoux, O. Carrillo, Estudio para la utilización de cenizas provenientes de la caldera cogeneradora Petropower en la estabilización de suelos, http://www2.udec.cl/~provial/trabajos_pdf/15ThenouxCenizasPetropower.pdf , Accessed date: 10 October 2017.
[10] N. Otero, A. Soler, Water Res. 36 (2002) 3989–4000.
[11] N. Otero, A. Soler, A. Canals, Appl. Geochem. 23 (2008) 1166–1185.
[12] J. Tenorio, D. Espinosa, Waste Manag. 21 (2001) 637–642.
[13] J. Esalah, M. Weber, J. Vera, Can. J. Chem. Eng. 78 (2000) 948–954.
[14] T. Alejo, M. Arruebo, V. Carcelen, V. Monsalvo, V. Sebastian, Chem. Eng. J. 309 (2017) 738–752.
[15] A. Bhattacharya, T. Naiya, S. Mandal, S. Das, Chem. Eng. J. 137 (2008) 529–541.
[16] A. Walcarius, L. Mercier, J. Mater. Chem. 20 (2010) 4478–4511.
[17] C. Gerardin, J. Rebo, M. Bonne, B. Lebeau, Chem. Soc. Rev. 42 (2013) 4217–4255.
[18] D. Li, H. Min, X. Jiang, X. Ran, L. Zou, J. Fan, J. Colloid. Interface Sci. 404 (2013) 42–48.
[19] X. Wu, L. Zhang, H. Ma, K. Yuan, Z. Li, J. Chin, Cer. Soc. 36 (2008) 269–270.
[20] C. Kresge, W. Roth, Chem. Soc. Rev. 42 (2013) 3663–3670.
[21] P. Tanev, T. Pinnavaia, Science 267 (1995) 865–867.
[22] X. Wu, H. Ma, L. Zhang, F. Wang, Appl. Surf. Sci. 261 (2012) 902–907.
[23] G. Fryxell, Y. Lin, Y.,H. Wu, Stud. Surf. Sci. Catal. 141 (2002) 583–589.
[24] Y. Lin, G. Fryxell, H. Wu, M. Engelhard, Environ. Sci. Technol. 35 (2001) 3962–3966.
[25] J. Lauwaert, E. De Canck, D. Esquivel, J. Thybaut, P. Van Der Voort, G. Marin, ChemCatChem 6 (2014) 255–264.
[26] Y. Zhao, Q. Gao, T. Tang, Y. Xu, D. Wu, Mater. Lett. 65 (2011) 1045–1047.
[27] M. Ghorbani, S. Mostafa, N. Ramezanian, F. Raji, Hydrometallurgy 161 (2016) 117–126.
[28] P. Tanev, J. Pinnavaia, Chem. Mater. 8 (1996) 2068–2079.
[29] T. Yokoi, T. Tatsumi, H. Yoshitake, J. Colloid Interface Sci. 274 (2004) 451–457.
[30] D. Lei, Q. Zheng, Y. Wang, H. Wang, J. Environ. Sci. 28 (2015) 118–127 China.
[31] Y. Yuan, W. Cao, W. Weng, J. Catal. 228 (2004) 311–320.
[32] B. Appa, Md Yakub, K. Chaitanya, N. Reddy, Indian J. Chem. Technol. 21 (2014) 188–198.
[33] A. Ali, P. Sherwood, Surf. Interface Anal. 29 (2000) 265–275.
[34] G. Fryxell, S. Mattigod, Y. Lin, H. Wu, S. Fiskum, K. Parker, F. Zheng, W. Yantasee, T. Zemanian, R. Addleman, J. Liu, K. Kenner, S. Kelly, X. Feng, J. Mater. Chem. 17 (2007) 2863–2874.
[35] W. Huang, Y. Zhang, D. Li, J. Environ. Manag. 193 (2017) 470–482.
[36] J. Zhang, Z. Shen, W. Shan, Z. Mei, W. Wang, J. Hazard Mater. 186 (2011) 76–83.
[37] J. Zhang, Z. Shen, Z. Mei, S. Li, W. Wang, J. Environ. Sci. 23 (2011) 199–205 China.
[38] G. Limousin, J. Gaudet, L. Charlet, S. Szenknect, V. Barthès, M. Krimissa, Appl. Geochem. 22 (2007) 249–275.
[39] H. Yoshitake, T. Yokoi, T. Tatsumi, Chem. Mater. 15 (2003) 1713–1721.
[40] S. Kelly, K. Kemner, G. Fryxell, J. Liu, S. Mattigod, K. Ferris, J. Phys. Chem. 105 (2001) 6337–6346.
[41] W. Chouyyok, R. Wiacek, K. Pattamakosan, T. Sangvanich, R. Grudzien, G. Fryxell, Environ. Sci. Technol. 44 (2010) 3073–3078.
[42] F. Li, L. Zhang, D. Evans, X. Duan, Colloid. Surface. 244 (2004) 169–177.
[43] B. Kannan, D. Higgins, M. Maryanne, M. Collinson, Langmuir 30 (2014) 10019–10027.
[44] J. Eng, I. Hubner, I.,J. Barriocanal, R. Opila, D. Doren, J. Appl. Phys. 95 (2004) 1963–1968.